Synthesis and Characterization of a New Ferrimagnetic Mixed-Valent Iron Fluorophosphate $[C_6N_4H_{21}][Fe^{III}_{3-x}Fe^{II}_xF_2(PO_4)(HPO_4)_2]_2$ ($x \sim 1.5$) with a Layered Structure

Sukhendu Mandal,[†] Srinivasan Natarajan,*[,†] Jean Marc Grenèche,[‡] Myriam Riou-Cavellec,[§] and Gérard Férey[§]

Framework Solids Laboratory, Chemistry and Physics of Materials Unit, Jawaharlal Nehru Centre for Advanced Scientific Research, Jakkur P.O., Bangalore 560 064, India, Laboratoire de Physique de l'Etat Condensé, UMR CNRS 6087, Université du Maine, Avenue O. Messiaen, 72085 Le Mans Cedex 9, France, and Institut Lavoisier, UMR CNRS 8637, Université de Versailles, 45, Avenue des Etats Unis, 78035 Versailles Cedex, France

Received May 7, 2002. Revised Manuscript Received July 22, 2002

The synthesis, structure, and magnetic properties of a mixed valent iron fluorophosphate, $[C_6N_4H_{21}][Fe^{III}_{3-x}Fe^{II}_xF_2(PO_4)(HPO_4)_2]_2$ ($x \sim 1.5$) has been described. The structure consists of a network of FeO_4F_2 octahedra and PO_4 tetrahedra linked through their vertexes, forming infinite two-dimensional sheets separated by the organic amine molecules, triethylenetetrammonium cations (TETA). A remarkable feature of this structure is the presence of chains of $Fe^{II}-O-Fe^{II}$ that are connected by Fe^{III} octahedra, forming infinite two-dimensional sheets of Fe−O/F−Fe. This is the first time such linkages have been observed in two-dimensional iron fluorophosphates. Magnetic studies indicate ferrimagnetic behavior with a Curie temperature of $T_c = 25$ K. Mössbauer studies show mixed occupancies in the Fe^{II} sites. Crystal data: $M = 567.61$, triclinic, space group = $P\bar{1}$ (no. 2), $a = 6.431(4)$ Å, $b = 10.274(5)$ Å, $c = 10.439(3)$ Å, $\alpha = 80.56(4)°$, $\beta = 89.53(2)°$, $\gamma = 87.94(4)°$, $V = 680.0(6)$ Å^3, $Z = 2$, $\rho_{(calc.)} = 2.772$ g cm^{-3}, μ(Mo Kα) = 3.610 mm^{-1}, $R_1 = 0.0634$ [1943 observed reflections with $I > 2\sigma(I)$].

Introduction

Although designing phases similar to the aluminosilicate zeolites continues to be one of the main driving forces for researchers in the area of open-framework materials, the discovery of new solids with novel structural features has also assumed an important role.[1] Among the many families of open-framework solids that have been synthesized and studied during the last 2 decades, the metal phosphates occupy a prime position. Of these, the transition-metal phosphates are important due to the interplay of several factors such as ligand-donor group geometry, coordination preferences, oxidation states of the metal ion, and so forth. In addition to these, the potential applications that would emerge by combining the magnetic properties of the transition metals with the channel structure adds impetus for research in the area of transition-metal phosphates, of which the iron phosphates constitute an important family.[2−10] Thus, iron phosphates with one-,[3] two-,[4−6] and three-dimensional[7−10] architectures have been synthesized and characterized.

The hydrothermal synthesis of open-framework iron phosphates generally employs simple salts of iron, such as chloride or nitrate, along with phosphoric acid, an

* To whom correspondence should be addressed. E-mail: raj@jncasr.ac.in. Fax: (+)91-80-846-2766.

[†] Jawaharlal Nehru Centre for Advanced Scientific Research.

[‡] Université du Maine.

[§] Université de Versailles.

(1) Cheetham, A. K.; Férey, G.; Loiseau, T. *Angew. Chem., Int. Ed.* **1999**, *38*, 3268, and references therein.

(2) Lii, K.-H.; Huang, Y.-F.; Zima, V.; Huang, C.-Y.; Lin, H.-M.; Jiang, J.-C.; Liao, F.-L.; Wang, S.-L. *Chem. Mater.* **1998**, *10*, 2599, and references therein.

(3) (a) Cavellec, M.; Riou, D.; Greneche, J.-M.; Férey, G. *Inorg. Chem.* **1997**, *36*, 2187. (b) Zima, V.; Lii, K.-H. *J. Chem. Soc., Dalton Trans.* **1998**, 4109. (c) Lethbridge, Z. A. D.; Lightfoot, P.; Morris, R. E.; Wragg, D. S.; Wright, P. A.; Kvick, Å.; Vaughan, G. *J. Solid State Chem.* **1999**, *142*, 455.

(4) (a) Cavellec, M.; Riou, D.; Férey, G. *J. Solid State Chem.* **1994**, *112*, 441. (b) Cavellec, M.; Riou, D.; Férey, G. *Eur. J. Solid State Inorg. Chem.* **1995**, *32*, 271; (c) Cavellec, M.; Riou, D.; Férey, G. *Acta Crystallogr.* **1995**, *C51*, 2242. (d) Cavellec, M. R.; Greneche, J. M.; Riou, D.; Férey, G. *Chem. Mater.* **1998**, *10*, 1914.

(5) (a) DeBord, J. R. D.; Reiff, W. M.; Haushalter, R. C.; Zubieta, J. *J. Solid State Chem.* **1996**, *125*, 186. (b) Lii, K.-H.; Huang, Y.-F. *Chem. Commun.* **1997**, 1311. (c) Zima, V.; Lii, K.-H.; Nguyen, N.; Ducouret, A. *Chem. Mater.* **1998**, *10*, 1914.

(6) (a) Mgaidi, A.; Boughzala, H.; Driss, A.; Clerac, R.; Coulon, C. *J. Solid State Chem.* **1999**, *144*, 163. (b) Cowley, A. R.; Chippindale, A. M.; *J. Chem. Soc., Dalton Trans.* **2000**, 3425.

(7) (a) Choudhury, A.; Natarajan, S.; Rao, C. N. R. *Chem. Commun.* **1999**, 1305. (b) Choudhury, A.; Natarajan, S. *Int. J. Inorg. Chem.* **2000**, *2*, 217. (c) Choudhry, A.; Natarajan, S. *J. Solid State Chem.* **2000**, *154*, 507.

(8) (a) Cavellec, M.; Riou, D.; Férey, G. *Inorg. Chim. Acta.* **1999**, *291*, 317. (b) Cavellec, M.; Riou, D.; Greneche, J.-M.; Férey, G. *J. Magn. Magn. Mater.* **1996**, *163*, 173. (c) Cavellec, M.; Riou, D.; Ninclaus, C.; Greneche, J.-M.; Férey, G. *Zeolites* **1996**, *17*, 250. (d) Cavellec, M.; Egger, C.; Linares, J.; Nogues, M.; Varret, F.; Férey, G. *J. Solid State Chem.* **1997**, *134*, 349. (e) Cavellec, M.; Greneche, J.-M.; Riou, D.; Férey, G. *Microporous Mater.* **1997**, *8*, 103. (f) Cavellec, M.; Greneche, J.-M.; Férey, G. *Microporous Mesoporous Mater.* **1998**, *20*, 45.

(9) (a) Lii, K.-H.; Huang, Y.-F. *Chem. Commun.* **1997**, 839. (b) Lii, K.-H.; Huang, Y.-F. *J. Chem. Soc., Dalton Trans.* **1997**, 2221. (c) Huanh, C.-Y.; Wang, S.-L.; Lii, K.-H. *J. Porous Mater.* **1998**, *5*, 147. (d) Zima, V.; Lii, K.-H. *J. Solid State Chem.* **1998**, *139*, 326.

(10) DeBord, J. R. D.; Reiff, W. M.; Warren, C. J.; Haushalter, R. C.; Zubieta, J. *Chem. Mater.* **1997**, *9*, 1994.

10.1021/cm0212008 CCC: $22.00
Published on Web 08/29/2002

organic amine, and a fluorinating agent. The introduction of fluoride ions, due to Kessler and co-workers,[11] strongly influences the formation of the framework solid, as exemplified by the synthesis of extra large pore gallophosphate, cloverite.[12] The F^- ion acts both as a mineralizer and as a connector between the metal atoms.[13] Recently, it was shown that the use of zinc complexes, in place of simple salts, in the starting synthesis mixture provides a facile route for the preparation of new types of open-framework zinc phosphates with novel architectures.[14] The metal complexes, probably, releases the metal ions slowly into the solution, during the hydrothermal crystallization, thereby facilitating the formation of such new structures. We have employed this approach for the preparation of novel iron phosphates, resulting in new open structures.[7b,7c] In continuation of this theme, we have been investigating the formation of iron phosphates using iron acetylacetonate, [Fe(acac)$_3$], as the starting source for iron in the presence of triethylenetetramine (TETA), employing hydrothermal methods. Our efforts were indeed successful and a new iron flurophosphate, $[C_6N_4H_{21}][Fe^{III}_{3-x}Fe^{II}_xF_2(PO_4)(HPO_4)_2]_2$ ($x \sim 1.5$), **I**, with a layered structure has been discovered by us. More importantly, the connectivity between the Fe(O/F)$_6$ octahedra forms an extended Fe−O/F−Fe infinite two-dimensional sheet, which is rather unusual. In this paper, we report the synthesis, structure, and magnetic properties of this interesting material.

Experimental Section

Synthesis. The iron fluorophosphate, $[C_6N_4H_{21}][Fe^{III}_{3-x}Fe^{II}_xF_2(PO_4)(HPO_4)_2]_2$ ($x \sim 1.5$), **I**, was synthesized under hydrothermal conditions starting from a coordination complex of Fe^{3+}, [Fe(acac)$_3$], as the source of iron. In a typical synthesis, 0.198 g of Fe(acac)$_3$ was dispersed in 2 mL of deionized water. To this, 0.14 mL of H_3PO_4 (85 wt %) and 0.08 mL of HF (48 wt %) were added under continuous stirring. Finally, 0.237 g of TETA was added to the above and the mixture was homogenized for 20 min at room temperature. The final orange-colored liquid with the composition 1:4:2:4:200 Fe(acac)$_3$:H_3PO_4:TETA:HF:H_2O (initial pH 4) was transferred and sealed in a 7-mL PTFE-lined stainless steel acid-digestion bomb and heated at 150 °C for 96 h. The final pH was 5.5. The resulting product contained large brownish red colored plates only and was vacuum-filtered and washed with plenty of deionized water and dried at ambient conditions. The brown color of the crystals suggested the possibility of a mixed valence for this iron compound. An EDAX analysis indicated an Fe:P ratio of 1:1, in addition to the presence of fluorine. A chemical analysis confirmed both the presence of fluorine (observed 6.5%, calculated 6.69%)[15] and the existence of two oxidation states for iron (Fe^{3+}/Fe^{2+} close to 1). The compound was characterized by powder X-ray diffraction (XRD), thermogravimetric analysis (TGA), and magnetic studies.

Thermogravimetric analysis was carried out in the temperature range 25−850 °C under a flow of nitrogen (50 mL/min). The studies show only one sharp mass loss with a tail. The total mass loss of 19.7% corresponds to the loss of some adsorbed water, amine molecule, and the condensation of the terminal hydroxyl group (calculated 19.2%). The calcined sample is amorphous.

Table 1. Crystal Data and Structure Refinement Parameters for Iron Fluorophosphate (I) $[C_6N_4H_{21}][Fe^{III}_{3-x}Fe^{II}_xF_2(PO_4)(HPO_4)_2]_2$ ($x \sim 1.5$)

formula mass	567.61
crystal system	triclinic
space group	$P\bar{1}$ (no. 2)
a (Å)	6.431(4)
b (Å)	10.274(5)
c (Å)	10.439(3)
α (deg)	80.56(4)
β (deg)	89.53(2)
γ (deg)	87.94(4)
V (Å^3)	680.0(6)
Z	2
T (K)	293
ρ_{calc} (g cm^{-3})	2.772
μ (mm^{-1})	3.610
F(000)	564
θ (deg)	1.98−23.31
indices	$-4 \le h \le 7$, $-11 \le k \le 11$, $-11 \le l \le 10$
reflections collected/unique	2915/1943 [$R_{int} = 0.0448$]
refinement method	full-matrix least-squares on $\|F^2\|$
data/restraints/parameters	1943/4/226
final R indexes [$I > 2\sigma(I)$]	$R_1 = 0.0634$[a], $wR_2 = 0.1573$[b]
min, max $\Delta\rho$ (e Å^{-3})	1.505 and −1.094

[a] $R_1 = \Sigma||F_o| - |F_c||/\Sigma |F_o|$. [b] $wR_2 = \{\Sigma[w(F_o^2 - F_c^2)^2]/\Sigma[w(F_o^2)^2]\}^{1/2}$. $w = 1/[\sigma^2(F_o)^2 + (aP)^2 + bP]$, $P = [\max(F_o^2,0) + 2(F_c)^2]/3$, where $a = 0.1137$ and $b = 0.0$.

Single-Crystal Structure Determination. A suitable single crystal was carefully selected under a polarizing microscope and glued to a thin glass fiber with cyanoacrylate (superglue) adhesive. Crystal structure determination by X-ray diffraction was performed on a Bruker-Siemens SMART-CCD diffractometer equipped with a normal focus, 2.4-kW sealed tube X-ray source (Mo Kα radiation, $\lambda = 0.71073$ Å) operating at 40 kV and 40 mA. A hemisphere of intensity data were collected at room temperature in 1321 frames with ω scans (width of 0.30° and exposure time of 10 s/frame) in the 2θ range of 3−46.5°. Pertinent experimental details for the structure determinations are presented in Table 1.

An absorption correction based on symmetry equivalent reflections was applied using the SADABS program.[16] Other effects, such as absorption by the glass fiber, were simultaneously corrected. The structures were solved and refined by the SHELXTL-PLUS suite of programs.[17] The direct methods solution readily revealed sufficient fragments of the structure (Fe, P, and O) and enabled the remainder of the non-hydrogen atoms to be located from difference Fourier maps. Fluorine atoms, identified by chemical analysis, were localized after consideration of thermal motion parameters and bond valence calculations.[18] All the hydrogen positions were initially located in the difference map and for the final refinement the hydrogen atoms were placed geometrically and held in the riding mode. Final residuals of $R_1 = 0.063$ and $wR_2 = 0.157$ were obtained for refinements with varying atomic positions for all the atoms and anisotropic thermal parameters for all non-hydrogen atoms and isotropic thermal parameters for all the hydrogen atoms. Full-matrix least-squares structure refinement against $|F^2|$ was carried out using the SHELXTL-PLUS[17] package of programs. The final atomic coordinates and selected bond distances and angles are presented in Tables 2−4.

Magnetization and ^{57}Fe Mössbauer Measurements. The magnetization (M) of the title compound was measured

(11) Guth, J. L.; Kessler, H.; Wey, R. *Stud. Surf. Sci. Catal.* **1986**, *28*, 121.
(12) Esterman, M.; McCusker, L. B.; Baerlocher, C.; Merrouche, A.; Kessler, H. *Nature (London)* **1991**, *352*, 320.
(13) Férey, G. *J. Fluorine Chem.* **1995**, *72*, 187.
(14) Neeraj, S.; Natarajan, S. *Int. J. Inorg. Mater.* **1999**, *1*, 317.
(15) *Vogel's Textbook of Quantitative Chemical Analysis*, 5th ed.; John Wiley & Sons Inc.: New York, 1989.
(16) Sheldrick, G. M. *SADABS Siemens Area Detector Absorption Correction Program*; University of Göttingen: Göttingen, Germany, 1994.
(17) Sheldrick, G. M. SHELXTL-PLUS *Program for Crystal Structure Solution and Refinement*; University of Göttingen: Göttingen, Germany, 1993.
(18) Teillet, J.; Varret, F. MOSFIT Program, unpublished.
(19) Brown, I. D.; Altermatt, D. *Acta Crystallogr. Sect.* **1985**, *B41*, 244.

Table 2. Final Atomic Coordinates (Å × 10^4) and Equivalent Isotropic Displacement Parameters (Å^2 × 10^3) for the Iron Fluorophosphate (I) $[C_6N_4H_{21}][Fe^{III}_{3-x}Fe^{II}_xF_2(PO_4)(HPO_4)_2]_2$ ($x \sim 1.5$)

atom	*x*	*y*	*z*	$U_{(eq)}$[a]
Fe(1)	2496(2)	4988(2)	5002(2)	15(1)
Fe(2)	7524(2)	4976(2)	10019(2)	17(1)
Fe(3)	5054(2)	2976(2)	7825(2)	12(1)
P(1)	5210(5)	2335(3)	5083(3)	17(1)
P(2)	5117(5)	2318(3)	10782(3)	19(1)
P(3)	10057(4)	3850(3)	7687(3)	11(1)
O(1)	2011(11)	2974(7)	7829(7)	15(2)
O(2)	8178(11)	2975(7)	7845(7)	12(2)
O(3)	5212(11)	1765(7)	9485(7)	17(2)
O(4)	5238(11)	1778(7)	6541(7)	16(2)
F(5)	5037(10)	4525(6)	8807(6)	26(2)
F(6)	4986(11)	4547(6)	6352(6)	29(2)
O(7)	2853(11)	6852(7)	5331(7)	20(2)
O(8)	3185(13)	3120(6)	4685(7)	20(2)
O(9)	19(11)	5278(7)	3674(6)	15(2)
O(10)	7036(12)	3085(7)	10977(7)	22(2)
O(11)	6916(12)	6878(7)	9072(7)	23(2)
O(12)	9997(11)	5233(7)	11277(6)	13(2)
O(13)	5345(13)	1114(7)	4372(7)	23(2)
O(14)	5101(13)	1070(7)	11886(8)	29(2)
N(1)	−191(15)	7639(8)	7164(9)	24(2)
C(1)	−290(22)	9032(9)	6496(11)	35(3)
C(2)	258(18)	10079(12)	7301(12)	43(4)
N(2)	−1286(16)	10259(10)	8346(9)	34(3)
C(3)	−730(23)	9594(11)	9688(11)	38(4)

[a] $U_{(eq)}$ is defined as one-third of the trace of the orthogonalized $\mathbf{U}_{ij}$ tensor.

Table 3. Selected Bond Distances for the Iron Fluorophosphate (I) $[C_6N_4H_{21}][Fe^{III}_{3-x}Fe^{II}_xF_2(PO_4)(HPO_4)_2]_2$ ($x \sim 1.5$)[a]

bond	distance (Å) [VB]	bond	distance (Å) [VB]
Fe(1)−O(7)	2.022(7) [0.459]	Fe(3)−F(5)	2.029(6) [0.388]
Fe(1)−O(8)	2.034(7) [0.444]	Fe(3)−F(6)	2.037(6) [0.380]
Fe(1)−O(9)	2.100(7) [0.372]	**Σ VB (Fe−O/F)**	**3.015**
Fe(1)−O(9)$^{\#1}$	2.115(7) [0.357]	P(1)−O(8)	1.530(8) [1.173]
Fe(1)−F(6)	2.129(7) [0.296]	P(1)−O(4)	1.536(8) [1.2445]
Fe(1)−F(6)$^{\#2}$	2.155(7) [0.276]	P(1)−O(7)$^{\#2}$	1.544(8) [1.218]
Σ VB (Fe−O/F)	**2.205**	P(1)−O(13)	1.558(8) [1.173]
Fe(2)−O(10)	2.068(7) [0.405]	**Σ VB (P−O)**	**4.8996**
Fe(2)−O(11)	2.065(7) [0.409]	P(2)−O(10)	1.520(8) [1.2997]
Fe(2)−O(12)	2.122(7) [0.350]	P(2)−O(11)$^{\#4}$	1.542(8) [1.2247]
Fe(2)−O(12)$^{\#3}$	2.111(7) [0.361]	P(2)−O(3)	1.552(8) [1.1921]
Fe(2)−F(5)	2.156(7) [0.286]	P(2)−O(14)	1.577(8) [1.1142]
Fe(2)−F(5)$^{\#4}$	2.142(7) [0.275]	**Σ VB (P−O)**	**4.8307**
Σ VB (Fe−O/F)	**2.087**	P(3)−O(1)$^{\#5}$	1.513(7) [1.3246]
Fe(3)−O(1)	1.957(7) [0.585]	P(3)−O(2)	1.523(8) [1.2892]
Fe(3)−O(2)	2.009(7) [0.509]	P(3)−O(12)$^{\#3}$	1.546(7) [1.2115]
Fe(3)−O(3)	1.962(7) [0.578]	P(3)−O(9)$^{\#2}$	1.551(7) [1.1953]
Fe(3)−O(4)	1.964(7) [0.575]	**Σ VB (P−O)**	**5.020**

[a] Values in brackets are the bond valences. Their sum SVB appears in bold type at the end of the list of the distances around every cation. Symmetry transformations used to generate equivalent atoms: (#1) $-x, -y+1, -z+1$; (#2) $-x+1, -y+1, -z+1$; (#3) $-x+2, -y+1, -z+2$; (#4) $-x+1, -y+1, -z+2$; (#5) $x+1, y, z$.

as a function of the applied field at many temperatures in the range 4−300 K with a Quantum Design Squid device. Mössbauer experiments were carried out at 300, 77, and 4.2 K by means of a bath cryostat, using a constant acceleration spectrometer and a Co source diffused in a Rh matrix. The values of the isomer shifts are quoted relative to α-Fe foil at 300 K. The hyperfine parameters were refined using a least-squares fitting procedure in the MOSFIT program.[19]

Results and Discussion

The asymmetric unit of the iron fluorophosphate, $[C_6N_4H_{21}][Fe^{III}_{3-x}Fe^{II}_xF_2(PO_4)(HPO_4)_2]_2$ ($x \sim 1.5$), **I**, contains 25 non-hydrogen atoms, of which 20 atoms belong to the "framework" and 5 atoms to the "guest" ammonium molecule. There are three crystallographically independent Fe and P atoms.

Table 4. Selected Bond Angles for the Iron Fluorophosphate (I) $[C_6N_4H_{21}][Fe^{III}_{3-x}Fe^{II}_xF_2(PO_4)(HPO_4)_2]_2$ ($x \sim 1.5$)[a]

moiety	angle (deg)	moiety	angle (deg)
O(7)−Fe(1)−O(8)	160.9(3)	O(4)−Fe(3)−F(6)	89.5(3)
O(7)−Fe(1)−O(9)	100.9(3)	O(2)−Fe(3)−F(6)	90.4(3)
O(8)−Fe(1)−O(9)	93.8(3)	F(5)−Fe(3)−F(6)	78.0(3)
O(7)−Fe(1)−O(9)$^{\#1}$	91.6(3)	O(8)−P(1)−O(4)	111.6(4)
O(8)−Fe(1)−O(9)$^{\#1}$	102.8(3)	O(8)−P(1)−O(7)$^{\#2}$	112.0(4)
O(9)−Fe(1)−O(9)$^{\#1}$	80.8(3)	O(4)−P(1)−O(7)$^{\#2}$	111.6(4)
O(7)−Fe(1)−F(6)	83.1(3)	O(8)−P(1)−O(13)	108.6(4)
O(8)−Fe(1)−F(6)	82.3(3)	O(4)−P(1)−O(13)	105.9(4)
O(9)−Fe(1)−F(6)	175.9(3)	O(7)$^{\#2}$−P(1)−O(13)	106.8(4)
O(9)$^{\#1}$−Fe(1)−F(6)	98.6(3)	O(10)−P(2)−O(11)$^{\#4}$	112.2(4)
O(7)−Fe(1)−F(6)$^{\#2}$	83.4(3)	O(10)−P(2)−O(3)	111.9(4)
O(8)−Fe(1)−F(6)$^{\#2}$	82.3(3)	O(11)$^{\#4}$−P(2)−O(3)	112.4(4)
O(9)−Fe(1)−F(6)$^{\#2}$	98.5(3)	O(10)−P(2)−O(14)	107.7(4)
O(9)$^{\#1}$−Fe(1)−F(6)$^{\#2}$	174.7(3)	O(11)$^{\#4}$−P(2)−O(14)	106.7(5)
F(6)−Fe(1)−F(6)$^{\#2}$	82.5(3)	O(3)−P(2)−O(14)	105.6(4)
O(11)−Fe(2)−O(10)	160.4(3)	O(1)$^{\#5}$−P(3)−O(2)	108.6(4)
O(11)−Fe(2)−O(12)$^{\#3}$	90.0(3)	O(1)$^{\#5}$−P(3)−O(12)$^{\#3}$	110.3(4)
O(10)−Fe(2)−O(12)$^{\#3}$	105.0(3)	O(2)−P(3)−O(12)$^{\#3}$	110.2(4)
O(11)−Fe(2)−O(12)	102.3(3)	O(1)$^{\#5}$−P(3)−O(9)$^{\#2}$	110.4(4)
O(10)−Fe(2)−O(12)	92.3(3)	O(2)−P(3)−O(9)$^{\#2}$	109.0(4)
O(12)$^{\#3}$−Fe(2)−O(12)	82.3(3)	O(12)$^{\#3}$−P(3)−O(9)$^{\#2}$	108.3(4)
O(11)−Fe(2)−F(5)$^{\#4}$	81.8(3)	Fe(3)−O(1)−P(3)$^{\#6}$	144.1(5)
O(10)−Fe(2)−F(5)$^{\#4}$	83.1(3)	Fe(3)−O(2)−P(3)	144.3(4)
O(12)$^{\#3}$−Fe(2)−F(5)$^{\#4}$	171.8(3)	Fe(3)−O(3)−P(2)	120.0(4)
O(12)−Fe(2)−F(5)$^{\#4}$	98.9(3)	Fe(3)−O(4)−P(1)	120.2(4)
O(11)−Fe(2)−F(5)	82.9(3)	Fe(3)−F(5)−Fe(2)$^{\#4}$	123.3(3)
O(10)−Fe(2)−F(5)	82.6(3)	Fe(3)−F(5)−Fe(2)	125.3(3)
O(12)$^{\#3}$−Fe(2)−F(5)	97.6(3)	Fe(2)$^{\#4}$−F(5)−Fe(2)	98.0(3)
O(12)−Fe(2)−F(5)	174.8(3)	Fe(3)−F(6)−Fe(1)	123.7(3)
O(5)$^{\#4}$−Fe(2)−F(5)	82.0(2)	Fe(3)−F(6)−Fe(1)$^{\#2}$	123.9(3)
O(1)−Fe(3)−O(3)	91.9(3)	Fe(1)−F(6)−Fe(1)$^{\#2}$	97.5(3)
O(1)−Fe(3)−O(4)	91.9(3)	Fe(1)−O(7)−P(1)$^{\#2}$	124.0(4)
O(3)−Fe(3)−O(4)	102.9(3)	Fe(1)−O(8)−P(1)	125.3(4)
O(1)−Fe(3)−O(2)	179.3(3)	Fe(1)−O(9)−P(3)$^{\#2}$	128.0(4)
O(3)−Fe(3)−O(2)	87.4(3)	Fe(1)$^{\#1}$−O(9)−P(3)$^{\#2}$	125.3(4)
O(4)−Fe(3)−O(2)	88.6(3)	Fe(1)−O(9)−Fe(1)$^{\#1}$	99.2(3)
O(1)−Fe(3)−F(5)	91.5(3)	Fe(2)−O(10)−P(2)	123.5(4)
O(3)−Fe(3)−F(5)	89.4(3)	Fe(2)−O(11)−P(2)$^{\#4}$	124.4(4)
O(4)−Fe(3)−F(5)	167.1(3)	Fe(2)$^{\#3}$−O(12)−P(3)$^{\#3}$	125.6(4)
O(2)−Fe(3)−F(5)	88.1(3)	Fe(2)−O(12)−P(3)$^{\#3}$	126.1(4)
O(1)−Fe(3)−F(6)	90.2(3)	Fe(2)−O(12)−Fe(2)$^{\#3}$	97.7(3)
O(3)−Fe(3)−F(6)	167.3(3)		

[a] Symmetry transformations used to generate equivalent atoms: (#1) $-x, -y+1, -z+1$; (#2) $-x+1, -y+1, -z+1$; (#3) $-x+2, -y+1, -z+2$; (#4) $-x+1, -y+1, -z+2$; (#5) $x+1, y, z$; (#6) $x-1, y, z$.

Of the three tetrahedrally coordinated P atoms, P(1) and P(2) make three P−O−Fe linkages and possess one terminal bond and P(3) makes four P−O−Fe connections. The P−O distances are in the range 1.513(8)−1.577(8) Å (average P(1)−O = 1.542 Å, P(2)−O = 1.548 Å, P(3)−O = 1.533 Å) and O−P−O bond angles are in the range 105.6(4)°−112.4(4)° (average 109.5°). The terminal P(2)−O(14) and P(1)−O(13) bonds with distances of 1.577(8) and 1.558(8) Å are P−OH linkages. One hydrogen position near each of the oxygen atoms O(13) and O(14) was observed in the difference Fourier maps. Similar P−O bond distances and bond angles have been routinely encountered in open-framework phosphates.[2−10] Bond valence sum calculations[18] also agree with the above.

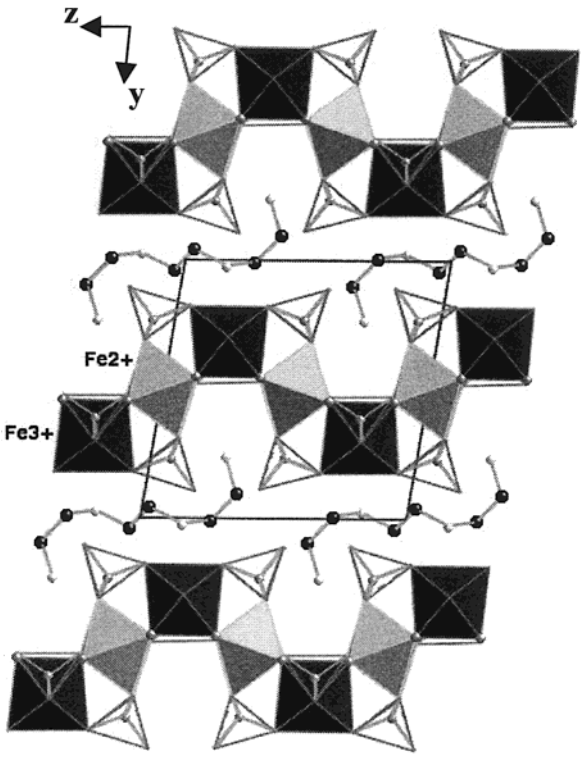

Figure 1. Structure of the iron fluorophosphate, $[C_6N_4H_{21}][Fe^{III}_{3-x}Fe^{II}_xF_2(PO_4)(HPO_4)_2]_2$ ($x \sim 1.5$), **I**, showing the Fe^{II} and the Fe^{III} ions.

The iron atoms are octahedrally coordinated by four oxygen atoms and two fluorine atoms with Fe−O/F distances in the range 1.957(7)−2.156(7) Å (average Fe(1)−O/F = 2.093 Å, Fe(2)−O/F = 2.111 Å, Fe(3)−O/F = 1.993 Å). The O/F−Fe−O/F bond angles are in the range 78.0(3)°−179.3(3)° (average O/F−Fe(1)−O/F = 106.2°, O/F−Fe(2)−O/F = 105.9°, O/F−Fe(3)−O/F = 106.2°). Of the 12 oxygen atoms, O(9) and O(12) are three-coordinated connecting Fe(1) and P(1) and Fe(2) and P(2), respectively. All of the three Fe atoms make four Fe−O−P bonds with an average Fe−O−P bond angle of 123.4°. The other two connections needed for the octahedral linkage comes from F bridges. While F(5) links Fe(2) and Fe(3), F(6) connects Fe(1) and Fe(3) and an average Fe−F−Fe bond angle of 115.3° results from such bonds. The complete list of bond distances and angles along with the bond valence sum (BVS) values is presented in Tables 3 and 4.

Bond valence sum calculations[18] indicate at first glance that, from the structural point of view, while Fe(3) is in +3 oxidation state, Fe(1) and Fe(2) are in a +2 state, (even if, for Fe(1), the valence sum is a little bit large), making this compound a mixed valent one. However, both the chemical analysis and the following Mössbauer study show that the situation is not so simple.

The structure of the iron fluorophosphate, $[C_6N_4H_{21}][Fe^{III}_{3-x}Fe^{II}_xF_2(PO_4)(HPO_4)_2]_2$ ($x \sim 1.5$), **I**, corresponds to the stacking of $[Fe^{III}_{3-x}Fe^{II}_xF_2(PO_4)(HPO_4)_2]_2$ layers along [010], between which amines are inserted (Figure 1). However, the framework can be understood also in terms of simpler building units, with two different types of description. First, the layer can be rebuilt from the edge-sharing of hexameric building units formed (Figure 2) by three phosphates and three iron octahedra. These SBU-6's were already encountered in ULM-12[8c] but, here, they are linked to each other by edges whereas, in ULM-12, vertexes were involved. In the second method of description, the mainly divalent iron octahedra, $Fe(1)O_4F_2$ and $Fe(2)O_4F_2$, are connected with the phosphate tetrahedra, $P(1)O_3(OH)$ and $P(2)O_3(OH)$, respectively, forming secondary building units (SBU) classified as SBU-4 by Férey (Figure 3a).[20,21] The SBU-4 units are connected through three-coordinated oxygen atoms [O(9) and O(12)], forming an infinite chainlike structure, which can be considered as a tetrahedrally decorated rutile-type chain, as shown in Figure 3b. The remaining $Fe(3)O_4F_2$ octahedra and $P(3)O_4$ tetrahedra are joined together to form a one-dimensional wire (Figure 3c). The two independent sets of chains shown in Figure 3b, formed by the linkages between $Fe(1)O_4F_2$ with $P(2)O_3(OH)$ and $Fe(2)O_4F_2$ with $P(1)O_3(OH)$ polyhedral units, are connected through these one-dimensional wires, giving rise to the layer structure. This is indeed a unique structure and this is the first time such a layer architecture has been observed in an iron fluorophosphate.

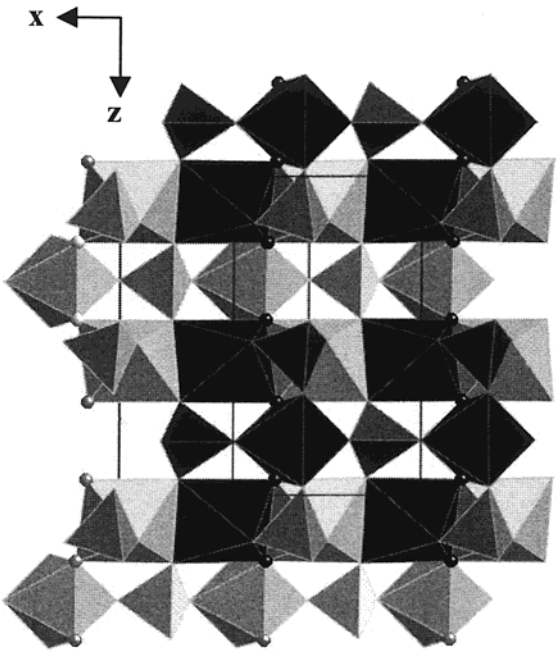

Figure 2. Structure of **I** in the *ac* plane showing a single layer and the hexameric SBU-6 building units.

What is remarkable about this iron fluorophosphate is the connectivity involving the iron octahedra. The two bivalent iron atoms, Fe(1) and Fe(2), independently are connected through three-coordinated oxygen atoms edge-wise, forming infinite Fe−O−Fe chains. The trivalent iron atom, Fe(3), connects the two chains, made from Fe(1) and Fe(2), respectively, through the Fe−F−Fe bonds, giving rise to an infinite sheet of Fe−O/F−Fe linkage in the *ac* plane (Figure 4). The position of Fe(3) (+3) is unique as it links two chains made from bivalent irons atoms. To our knowledge, this is the first time such an Fe−O/F−Fe linkage has been observed in

(20) Cavellec, M.; Riou, D.; Ninclaus, C.; Grenèche, J. M.; Férey, G. *Zeolites* **1996**, *17*, 250.
(21) Férey, G. *J. Solid State Chem.* **2000**, *152*, 37.

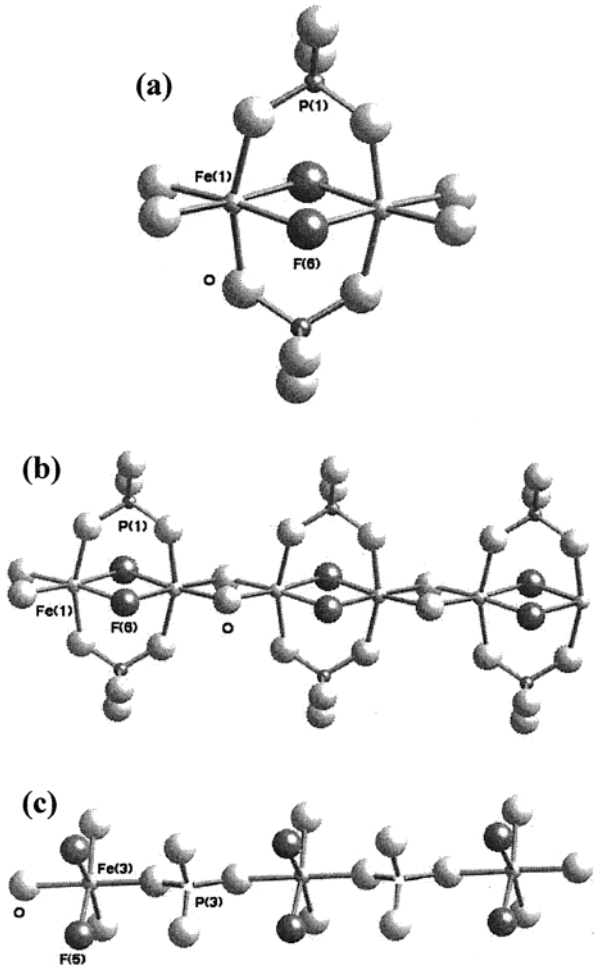

Figure 3. (a) The secondary building unit, SBU-4. This unit has a site symmetry of −1. (b) Figure showing the connectivity between the SBU-4 units, through the three-coordinated oxygen atoms (see text). (c) The one-dimensional chain unit formed by the linkages between FeO_4F_2 and PO_4 units.

a two-dimensional iron fluorophosphate. The layer arrangement in the *bc* plane shows a large number of hydrogen bond interactions, typical of lower dimensional solids (Figure 5). Thus, strong N−H···O and relatively weaker C−H···O hydrogen bonds have been observed in the iron fluorophosphate, in addition to the interlayer O−H···O interactions involving the terminal P−OH linkages. The interlayer O−H···O hydrogen bonds form pseudo channels. It has been shown earlier that the hydrogen bond interactions are important for the structural stability of lower dimensional solids.[4−6] The complete list of hydrogen bond interactions is listed in Table 5.

Even if the structural results indicate a tendency to $Fe^{2+}-Fe^{3+}-Fe^{2+}$ cationic ordering within the plane, the chemical analysis (1:1 ratio between $Fe^{2+}-Fe^{3+}$) is not in agreement with the expected 2:1 one and seems to indicate cationic disorder to some extent. The results of the Mössbauer study confirm this assessment. Indeed, if a strict cationic order exists, the Mössbauer spectrum must exhibit three different contributions in equal proportions 1:1:1: one for Fe^{3+} and two different ones for Fe^{2+} since, for the latter, the octahedra do not exhibit the same distortion. After the fitting procedure (Table 6), three contributions indeed appear at 300 K, all corresponding to high spin configurations for iron ions,

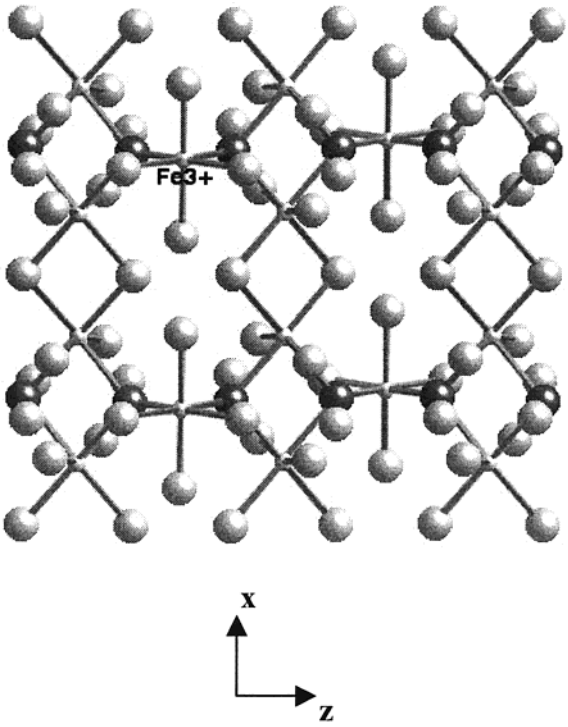

Figure 4. Figure showing the connectivity between the Fe^{II} chains and Fe^{III}.

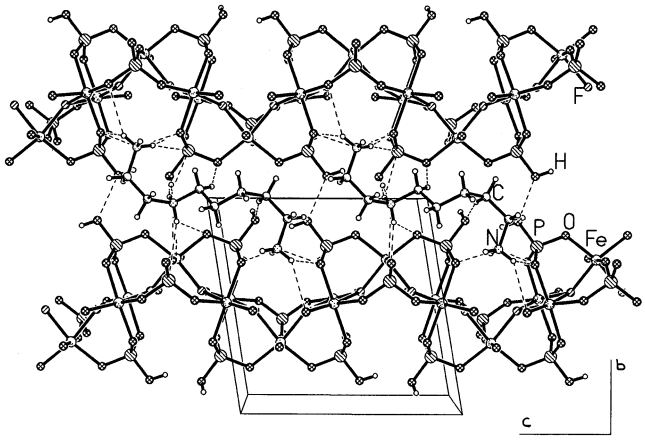

Figure 5. Structure of **I** in the *bc* plane showing the layer arrangement. Dotted lines represent the various hydrogen bond interactions.

Table 5. Important Hydrogen Bond Interactions in the Iron Fluorophosphate (I) $[C_6N_4H_{21}][Fe^{III}_{3-x}Fe^{II}_xF_2(PO_4)(HPO_4)_2]_2$ ($x \sim 1.5$)

D−H···A	D−H (Å)	H···A (Å)	D···A (Å)	D−H···A (deg)
N(1)−H(2)···O(11)	0.89	1.88	2.752(2)	163
N(1)−H(8)···O(10)	0.89	2.03	2.813(2)	147
N(2)−H(8)···O(2)	0.90	1.89	2.763(1)	163
N(2)−H(9)−O(14)	0.89	2.01	2.881(1)	164
O(14)−H(29)···N(2)	0.82	2.07	2.881(2)	173
O(13)−H(39)···O(14)[a]	0.82	1.85	2.609))	152
C(1)−H(4)···O(13)	0.97	2.47	3.397(2)	159
C(2)−H(6)···O(14)	0.97	2.30	3.238(1)	162
C(3)−H(11)···O(3)	0.97	2.46	3.295(1)	144

[a] Intralayer.

but with proportions different from the expected value (Figure 6a). Indeed, the percentage of Fe^{3+} deduced from the large doublet is close to 50% instead of 33% while one of the contributions of Fe^{2+} is abnormally low (21% instead of 33%). This means that the ratio between Fe^{2+}

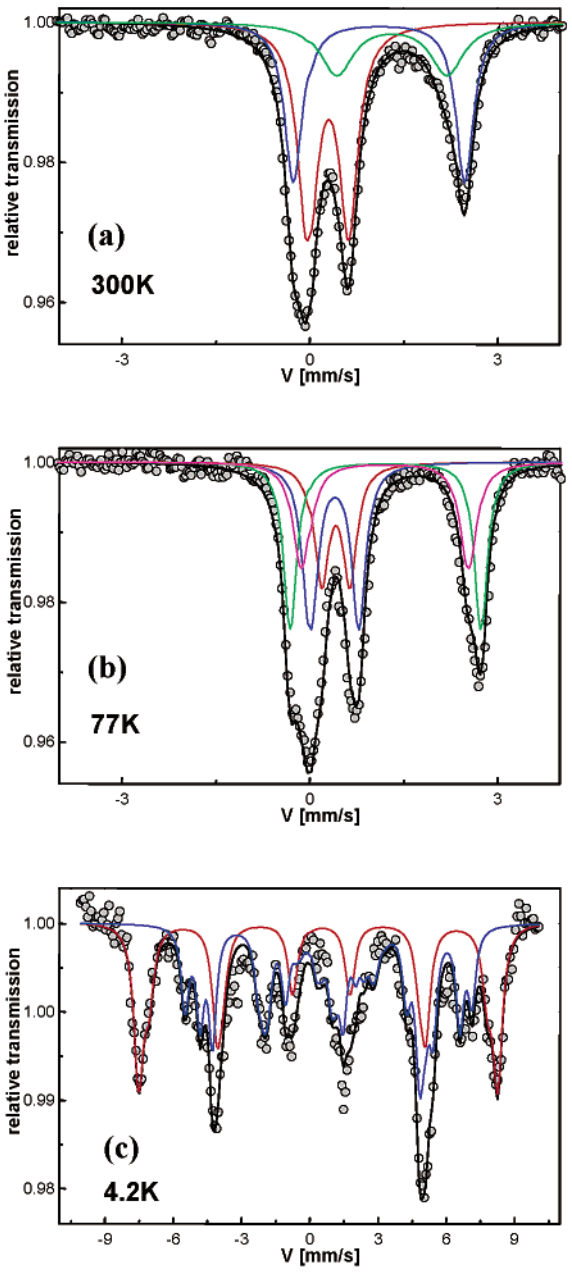

Figure 6. Mössbauer spectra of **I** (a) at 300 K, (b) at 77 K, and (c) at 4.2 K.

Table 6. Hyperfine Parameters at 300 and 77 K (I.S., Isomer Shift; G, Line Width at Half-Height; SQ, Quadrupolar Splitting; %, Proportion of Each Component)

T (K)	mode	I.S. (mm/s) ±0.02	Γ (mm/s) ±0.02	SQ (mm/s) ±0.02	% ±5
300	**Σ1(3+)**	0.42	0.178	0.635	45%
	Σ2(2+)	1.24	0.169	2.705	34%
	Σ3(2+)	1.26	0.318	1.758	21%
77	**Σ1(3+)**	0.52	0.27	0.76	28%
	Σ1a(3+)	0.53	0.27	0.45	21%
	Σ2(2+)	1.34	0.26	3.02	28%
	Σ3(2+)	1.33	0.33	2.64	23%

and Fe^{3+} is closer to 1:1 than 2:1, in agreement with the chemical analysis, and therefore implies the presence of Fe^{3+} on the corresponding sites of Fe^{2+}. In particular, one Fe^{2+} site is more affected that the other (Table 6), indicating a preferential substitution on this site. This means also that the presence of Fe^{3+} on this site must correspond to a second contribution of Fe^{3+} on the spectrum (Figure 6b), which is revealed at 77 K after a fit with four contributions: two of Fe^{2+} (28 and 23%) and two of Fe^{3+} (28 and 21% with an esd of 5%). Within one esd, the situation can be described within two limits, which both imply the full occupancy of the Fe(3) site by Fe^{3+} (see the following table). The first

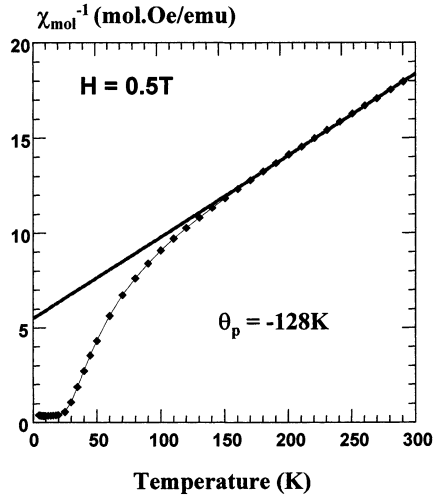

Figure 7. $\chi-T$ plot of **I** showing typical ferrimagnetic behavior.

Fe(3) site		Fe(2) site	Fe(1) site
Fe^{3+} 33%	Fe^{3+} on site Fe(1): 16%	Fe^{2+} 33%	$Fe^{2+} + Fe^{3+}$ 18% + 16%
Fe^{3+} 33%	Fe^{3+} on sites Fe(2) and Fe(1): 16%	$Fe^{2+} + Fe^{3+}$ 28% + 5%	$Fe^{2+} + Fe^{3+}$ 23% + 11%

corresponds to a mixed valence only on the Fe(1) site and the second to a distribution of Fe^{3+} over the two Fe^{2+} sites by taking the experimental value of their occupation. This is in agreement with the VBA analysis of Fe^{2+} in Table 3 for the assignation of the sites.

From the Mössbauer results, it is therefore clear that the true formula of the title solid is $[C_6N_4H_{21}][Fe^{III}_{3-x}Fe^{II}_xF_2(PO_4)(HPO_4)_2]_2$ ($x \sim 1.5$). Finally, the Mössbauer spectrum at 4.2 K was measured but found to be too complicated (Figure 6c) to interpret accurately. The fit, realized with five contributions, gave 45(5):55(5) for the Fe^{3+}/Fe^{2+} ratio, in fair agreement with the measurements performed at higher temperatures.

Whatever the exact composition of the solid, the existence of mixed valence induces the possibility of interesting magnetic properties. The $\chi^{-1}(T)$ curve of Figure 7 is characteristic of ferrimagnetic behavior with a θ_p (−128 K), indicative of medium antiferromagnetic interactions; $M(H)$ curves (Figure 8) are typical of ferri- or ferromagnetic behavior, but the value of the magnetization at high fields (3.3 μB/mol [6 Fe]) is in good agreement with the proposed repartition of cations ($3 \times 5\,\mu B - 3 \times 4\,\mu B = 3\,\mu B$/mol). The Curie temperature (T_c 25(1) K) was accurately determined by the thermal evolution of the FC and ZFC curves at 0.01 T (insert of Figure 8). Moreover, the title compound exhibits (Figure 9) a very large hysteresis loop at 4.5 K (H_c = 2300 Oe and M_r = 2.3 μB/mol).

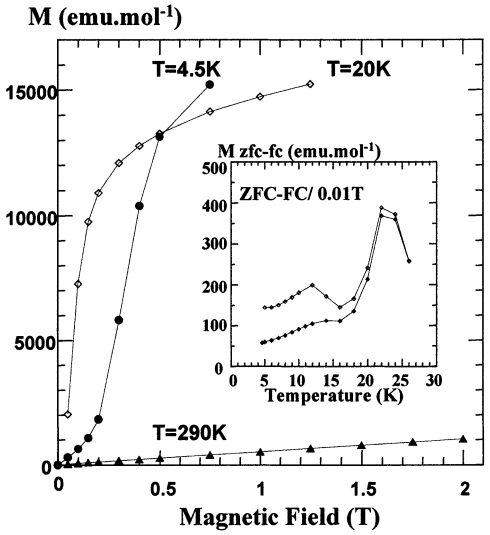

Figure 8. *M* vs *H* plot of **I** as a function of temperature. Insert shows the FC and ZFC curves.

Finally, coming back to synthesis, it is interesting to note that this experiment provides one of the rare examples of mixed valence in the chemistry of iron phosphates. The starting material contained only Fe(III) and the result is a mixed valence with a 1:1 ratio between iron species. Several things can be responsible for this fact: the value of the pH, which favors the existence of Fe^{2+}; the reducing effect of TETA; and, perhaps, the peculiar behavior of acac. The studies of different systems corresponding to close experimental conditions are currently on the way to find other mixed valence iron phosphates.

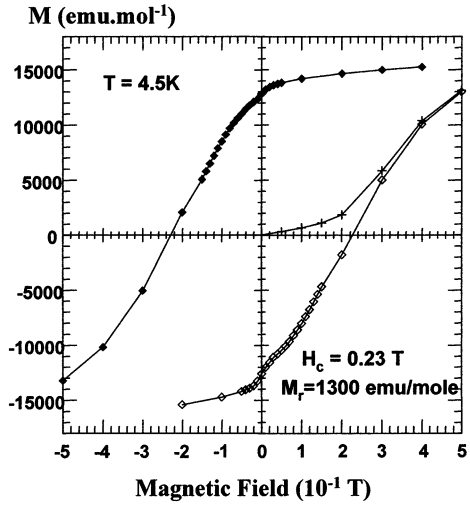

Figure 9. *M* vs *H* hysteresis studies at 4.5 K showing the large hysteresis.

Acknowledgment. S.M. and S.N. thank Prof. C. N. R. Rao, FRS, for his support and encouragement. S.N. thanks the Department of Science and Technology (DST), Government of India, for the award of a research grant.

Supporting Information Available: X-ray crystallographic data (CIF). This material is available free of charge via the Internet at http://pubs.acs.org.

CM0212008